# AlN Precipitation During Isothermal Annealing of Ultra Low Carbon Steel

**Rene Radis[1,2)]*, Sabine Schwarz[3)], Sabine Zamberger[4)], and Ernst Kozeschnik[1)]**

[1)] Christian Doppler Laboratory 'Early Stages of Precipitation', Institute of Materials Science and Technology, Vienna University of Technology, Favoritenstraße 9-11, 1040 Vienna, Austria
[2)] Institute for Materials Science and Welding, Graz University of Technology, Kopernikusgasse 24, 8010 Graz, Austria
[3)] University Service Centre for Transmission Electron Microscopy, Vienna University of Technology, Wiedner Hauptstraße 8-10/052, 1040 Vienna, Austria
[4)] Voestalpine Stahl Donawitz GmbH & Co KG, Kerpelystraße 199, 8700 Leoben, Austria
* Corresponding author; e-mail: rene.radis@tugraz.at

The precipitation of AlN is investigated in the austenite region of ultra low carbon steel. The evolution of the size and the morphology of AlN precipitates are studied by transmission electron microscopy (TEM) after isothermal annealing for different times at temperatures of 950 °C and 1050 °C. Various different morphologies are observed, including cuboids, large plates as well as irregular structures. In addition to the experimental analysis, thermo-kinetic simulations are carried out with the software package MatCalc. The numerically calculated evolution of the mean radii as well as the time-temperature-precipitation (TTP) diagram for AlN precipitation in the present alloy show good agreement with experiment.

**Keywords:** AlN, grain boundary precipitation, precipitation kinetics, ultra low carbon steel

Submitted on 3 December 2010, accepted on 8 March 2011

## Introduction

In addition to the importance of Al for the deoxidation of steel during casting, this element plays an important role as microalloying element. Similar to Ti and Nb, Al shows a very high affinity to N, often forming AlN precipitates already in the austenite region of microalloyed steel [1]. Because of considerable volumetric misfit between the AlN precipitates and the steel matrix, the precipitation of AlN in austenite occurs predominantly at grain boundaries [2–7]. Thus, Speich et al. [8] suggested, that, apart from Ti additions, Al is maybe the most effective element for avoiding austenite grain coarsening [9–11] at high temperatures. The austenite grain size directly influences mechanical and technological properties, such as hot ductility [12–14], impact toughness [14], deep drawability [15] or weldability [16]. On the other hand, precipitation of AlN can cause embrittlement and induce cracking phenomena, such as, e.g. rock candy fracture [17–23]. Some authors [24] report that AlN without any other trace element has no influence on hot ductility of high purity iron.

The equilibrium crystallographic structure of AlN is the hexagonal wurtzite structure with a lattice constant of $a = 0.311$ nm and $c = 0.498$ nm. In the early stages of precipitation, also, a cubic structure with $a = 0.412$ nm is observed [25–27]. A detailed investigation of the two crystallographic structures can be found in Ref. [28].

AlN precipitates in steel cover a wide range of different morphologies. Depending on the amount of alloying additions (especially Al and N), heat treatment and processing history, AlN precipitates can occur as dendrites (up to several hundred microns in length), large plates, rods and needles, rectangular, cubical, or as finely dispersed spherical particles. An overview of all the different morphologies of AlN in steel, obtained by numerous experimental investigations, can be found in the extensive review of Wilson and Gladman [16].

A high number of experimentally obtained kinetic data is reported in literature as well as several theoretical treatments of AlN precipitation. A summary of these can be found in Ref. [29], where a comprehensive and rigorous description of the precipitation kinetics of AlN in microalloyed steel is presented. In this work, the fact is accounted for that AlN precipitation can occur simultaneously at grain boundaries and on dislocations, depending on chemical composition, grain size and annealing temperature. However, since the available experimental data on AlN precipitation are determined mainly by indirect methods, e.g. the Beeghly method [30], no information is provided on the size and morphology of precipitates along with the kinetic information during isothermal annealing of undeformed microalloyed steel.

This task is performed in the present work, where the evolution of the size and the morphology of AlN precipitates are studied by transmission electron microscopy (TEM) after isothermal annealing at temperatures of 950 °C and 1050 °C for different holding times. Moreover, utilizing a new model for precipitation at grain boundaries [31], which is implemented in the thermo-kinetic software MatCalc [32–34], computer simulations on AlN precipitation are carried out, according to the procedure presented in Ref. [29]. The evolution of the mean radii as well as a time-temperature-

  

precipitation (TTP) diagram for AlN formation in the austenite region of the present alloy are calculated and compared to the experimental data obtained by the TEM analysis.

## Experimental

**Material and Heat Treatment.** For the present investigations, an ultra low carbon model alloy is used, which was cast in a vacuum furnace under argon overpressure. The chemical composition is analyzed by spark emission spectroscopy. The results are given in **Table 1**.

To ensure a homogenous initial microstructure for the subsequent isothermal annealing experiments, several preheat and deformation treatments are carried out. After casting, the alloy is deformed at approximately 1100 °C using two different deformation rates of 0.4 and 0.7 before and after turning the material by 90°. Afterwards, the material is heated to 1000 °C, held for 1200 s, and then air cooled to room temperature to stimulate allotropic transformations. This heat treatment is repeated two times, ensuring that the initial dendritic microstructure after casting transforms into a homogenous bulk volume. Furthermore, the ingot is soaked at a temperature of 1380 °C for 3600 s and then quenched into water, thereby dissolving the AlN precipitates developed during the production procedure of the alloy. The entire heat treatment after casting is carried out in ambient atmosphere and decarburization of the surface layer is expected. Thus, the surface area is analyzed by light microscopy with special emphasis on decarburization, and 3 mm of the surface are removed mechanically.

The ingot is cut into pieces with $4 \times 4 \times 13$ mm, which are heat treated in a high speed quenching dilatometer under vacuum atmosphere, according to **Fig. 1**. After heating to 1380 °C with a heating rate of 50 $Ks^{-1}$, the samples are kept on this level for 20 s to dissolve precipitates, which formed temporarily before reheating. Then, the samples are quenched to two different temperatures of 1050 °C and 950 °C, held for several different annealing times, and then quenched to room temperature. Temperature is controlled with Pt-Pt/Rh 10% (Typ S) thermo couples. Helium is used for the quenching treatments.

**Electron Microscopy.** Transmission electron microscopy (TEM) investigations are carried out on a FEI TECNAI F20 TEM operated at 200kV accelerating voltage. The TEM samples are cut and ground to discs of 200 μm thickness and 3 mm diameter for etching. The electro polishing procedure is carried out on a Struers Tenupol-5 with 10% perchloric acid and 90% methanol. The etching temperature was about -5°C to -8°C, and the etching voltage

**Table 1.** Chemical composition (wt%) of the investigated alloy determined by emission spectroscopy.

| C | Si | Mn | Al | N | S | Fe |
|---|---|---|---|---|---|---|
| 0.002 | 0.039 | 0.371 | 0.14 | 0.0044 | 0.0059 | bal. |

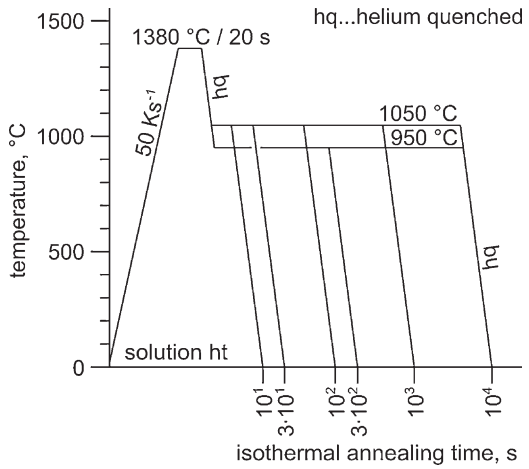


**Figure 1.** Heat treatments used for the present investigations.

varied between 24V and 28V. After the etching process the samples are cleaned with 50% butyl-alcohol and 50% etyl-alcohol.

For determining the size and morphology of the AlN precipitates, TEM micrographs are recorded and selected area electron diffraction (SAD) is used for phase analysis. The chemical composition of the precipitates is analysed using energy dispersive X-ray analysis (EDX).

## Simulation

For the thermo-kinetic simulations, the software package MatCalc [32–34] (version 5.41) and the corresponding databases 'mc_steel' [35] and 'mc_sample_fe' [36] are used. In this approach, the nucleation kinetics of precipitates is calculated from Classical Nucleation Theory (CNT) [37, 38] extended for multi-component systems [32, 37, 39]. Accordingly, the transient nucleation rate $J$ is given as

$$J = N_0 Z \beta^* \cdot \exp\left(\frac{-G^*}{k \cdot T}\right) \cdot \exp\left(\frac{-\tau}{t}\right). \quad (1)$$

$J$ describes the rate, at which nuclei are created per unit volume and time. $N_0$ represents the total number of potential nucleation sites. The Zeldovich factor $Z$ takes into account that the nucleus is destabilized by thermal excitation as compared to the inactivated state. The atomic attachment rate $\beta^*$ takes into account the long-range diffusive transport of atoms, which is needed for nucleus formation if the chemical composition of the matrix is different from that of the precipitate. $T$ is the temperature, $k$ the Boltzmann constant, $\tau$ the incubation time and $t$ the time. The critical energy for nucleus formation $G^*$ is

$$G^* = \frac{16\pi}{3} \frac{\gamma^3}{(\Delta G_{vol} - \Delta G_s)^2}, \quad (2)$$

with the interfacial energy $\gamma$, the volume free energy change $\Delta G_{vol}$ and the misfit strain energy $\Delta G_s$. The interfacial energy is calculated using the generalized broken-bond

  

approach [40], assuming a planar and sharp interface. Corrections for the small size of the precipitate are taken into account according to Ref. [41]. It is important to note that $G^*$ is a most essential quantity in nucleation theory, when compared to the other quantities occurring in equation (1). Since $G^*$ appears in the exponent of the nucleation rate equation (1), small changes in $\gamma$ and/or $\Delta G_{vol}$-$\Delta G_s$ can lead to huge variations in $J$, which has been demonstrated recently for $\gamma$'-precipitation in a Ni-base superalloy [42].

Once a precipitate is nucleated, its further growth is evaluated based on the evolution equations for the radius and composition of the precipitate derived by Svoboda et al. [32] in a mean-field approach, utilizing the thermodynamic extremal principle. Accordingly, the growth rate $\dot{\rho}_k$ and the rate of change of chemical composition $\dot{c}_{ki}$ of the precipitate with index $k$ are obtained from solution of the linear system of equations

$$A_{ij}y_j = B_i, \tag{3}$$

where the variable $y_j$ represents the rates $\dot{\rho}_k$ and $\dot{c}_{ki}$, as well as the Lagrange multipliers from the stoichiometry constraints (see Ref. [32]).

The system of equations (3) is solved for each precipitate $k$ separately. The full expressions for the coefficients $A_{ij}$ and $B_i$, as used in the present work, are given in Ref. [34]. The numerical time integration of $\dot{\rho}_k$ and $\dot{c}_{ki}$ is performed in the software MatCalc, based on the classical numerical Kampmann – Wagner approach [43], and it is described in detail in Ref. [33]. In addition to the classical treatment of randomly distributed precipitates as developed in Ref. [32], the present calculations utilize a novel model [31] for the evolution of grain boundary precipitates.

Using this computational approach and the simulation methodology developed in Ref. [29], the evolution of the mean radii as well as an isothermal time-temperature-precipitation (TTP) diagram are calculated for AlN precipitation in the austenite region of the present alloy. In addition to the numerical model briefly presented before, several physical effects are considered, among them are the precipitate/matrix volumetric misfit and the temperature dependent Young's modulus, composition-, temperature- and size-dependent interfacial energies, as well as the ratio between bulk and grain boundary diffusion. Precipitation of AlN is assumed to occur simultaneously at grain boundaries and dislocations. For this reason, two separate populations of AlN precipitates are considered in the simulations, differing in the type of nucleation site and the value for the volumetric misfit, 27%[1] and 0%, for precipitation at dislocations and grain boundaries, respectively. A dislocation density of $10^{11}$ m$^{-2}$ (Ref. [44]) and an estimated mean grain diameter of 300 $\mu$m are assumed for annealed austenite. Additional simulation details are described in detail in Ref. [29] and shall not be repeated here.

[1] The effective volume misfit of AlN at dislocations, originally determined with 0.19 in Ref. [29] must be replaced by 0.27 when using MatCalc versions 5.40 and higher. The misfit value has erroneously been taken twice in older versions.

## Results

**Figs. 2 (a)** and **3(a)** show the calculated evolution of the mean radii of AlN precipitates during holding at temperatures of 1050 °C and 950 °C, respectively. At these temperatures, precipitation is predicted to occur only at grain boundaries. Precipitation at dislocations is effectively suppressed by the volumetric misfit between AlN and the austenite matrix. Micrographs obtained by TEM investigations after isothermal annealing times of 100, 1000, 10000 s at 1050 °C and 300, 1000, 10000 s at 950 °C are shown in Figs. 2(b-f) and 3(b-f). With the exception of the shortest annealing times, two micrographs of each sample with different precipitates are presented. No AlN precipitates could be confirmed at annealing times of 10 and 30 s in the case of T = 1050 °C and 10 and 100 s in the case of T = 950 °C. The AlN precipitates cover a wide range of different morphologies. Figs. 2(b,e) and 3(c,d) show cuboids, whereas Figs. 2(c,d) and 3(f) show large thin plates. Also, irregular structures are observed, see Figs. 2(f) and 3(b,e).

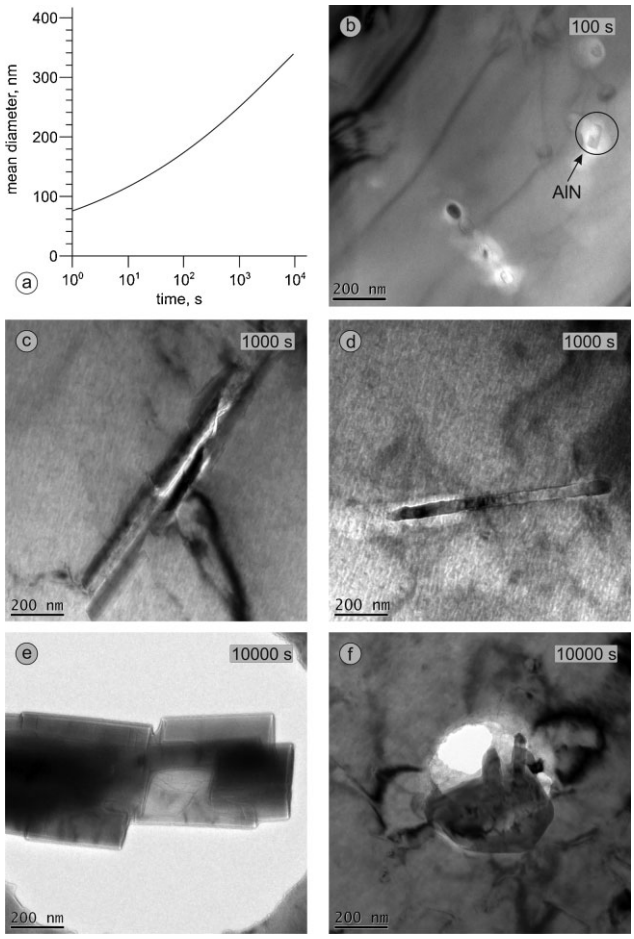


**Figure 2.** Calculated mean diameter of spherical AlN precipitates at 1050 °C (a) and corresponding TEM micrographs obtained after holding for different times (b-f).

  

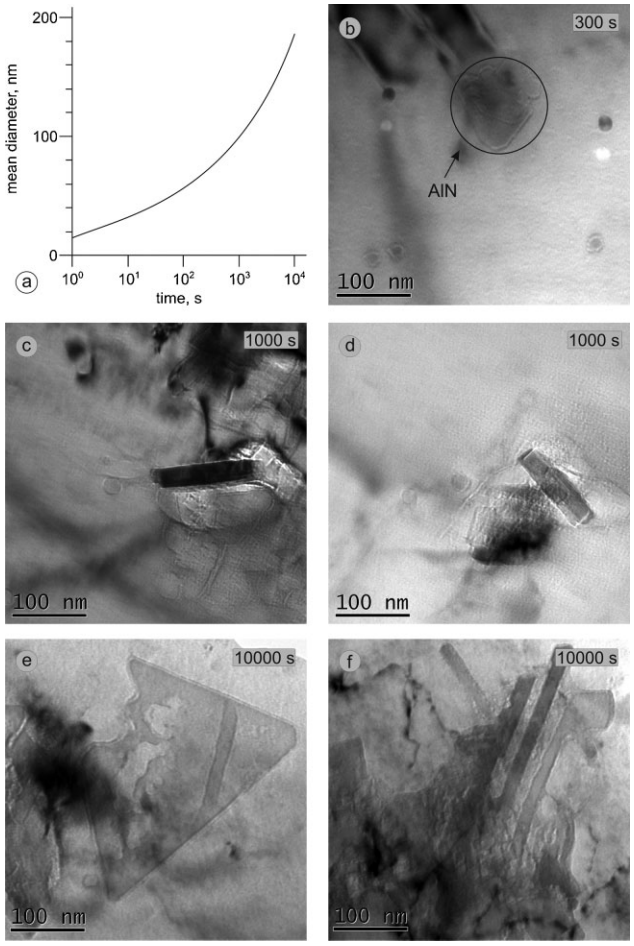


**Figure 3.** Calculated mean diameter of spherical AlN precipitates at 950 °C (a) and corresponding TEM micrographs obtained after holding for different times (b-f).

In addition to the AlN precipitates, MnS particles are observed already after short annealing times, see Figs. 2(b) and 3(b). Apart from these small spherical MnS, all precipitates in Figs 2 and 3 are clearly identified as AlN using the EDX technique.

**Fig. 4** shows exemplarily an EDX spectrum for AlN, determined after isothermal annealing at 1050 °C for 1000 s. Next to the iron peaks of the matrix, characteristic peaks for Al and N are detected, clearly indicating the presence of AlN. Additionally, selected area electron diffraction analysis confirms the crystallographic structure of AlN, see **Fig. 5**. **Table 2** shows the comparison of the measured spot distances with those calculated for AlN with hexagonal wurtzite structure, using the lattice parameters a = 0.311 nm and c = 0.498 nm [45].

**Fig. 6** shows the predicted [29] time-temperature-precipitation (TTP) diagram for AlN precipitation in the austenite region of the investigated alloy and the comparison with experimental data obtained by TEM investigations. The solid and the dashed lines represent 5% and 95% of the relative phase fraction of AlN precipitated at grain boundaries and at dislocations, respectively. No nucleation

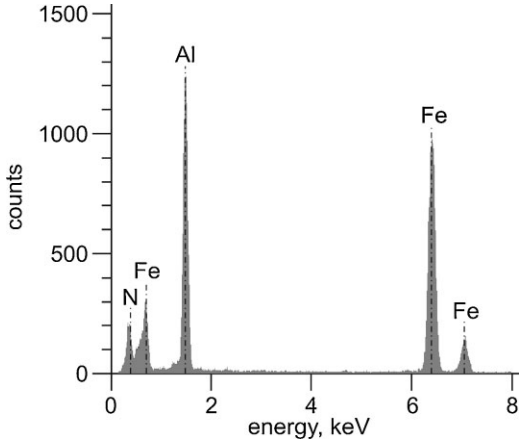


**Figure 4.** EDX spectrum of AlN precipitate determined after isothermal annealing at 1050 °C for 1000 s.

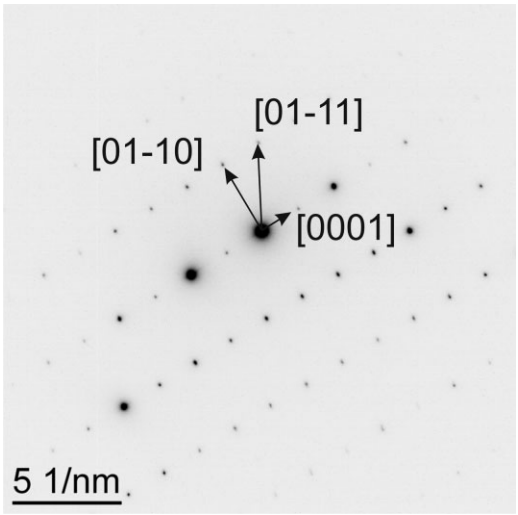


**Figure 5.** Diffraction pattern of the phase AlN in zone axis [2,-1,-1,0] in a specimen annealed at 1050 °C for 1000 s.

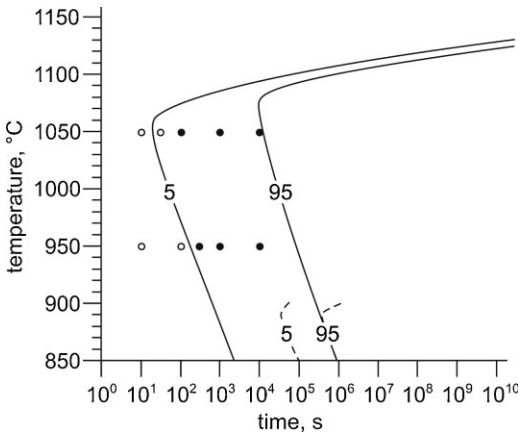


**Figure 6.** Calculated time-temperature-precipitation (TTP) diagram of AlN in austenite for the investigated alloy and comparison with experimental data.

  

**Table 2.** Comparison between measured and calculated spot distances for indexing the diffraction pattern in Fig. 5.

| (hkl) | Measured distance [nm] | Calculated distance [nm] |
|---|---|---|
| 001 | 1.99 | 2.01 |
| 010 | 3.63 | 3.71 |
| 011 | 4.17 | 4.22 |

at dislocations is predicted for temperatures higher than 900 °C, where the isothermal heat treatments are carried out. The filled circles stand for experimental data, where AlN precipitates are clearly detected, whereas the unfilled circles indicate experiments, where no AlN precipitates could be detected.

## Discussion

The TEM investigations confirm a wide range of different morphologies of AlN precipitates, which is in accordance with the data reported in the extensive review of Wilson and Gladman [16]. Unfortunately, no experimental information can be provided, as to whether the precipitates are nucleated at grain boundaries or at dislocations, since the austenite matrix transforms to ferrite during cooling to room temperature. However, it is well established, that in the austenite region of undeformed, well annealed microalloyed steel, precipitation of AlN occurs predominantly at austenite grain boundaries, see e.g. Refs. [2–7]. Moreover, a theoretical treatment was presented recently [29, 31], where precipitation of AlN is treated simultaneously at grain boundaries and at dislocations. In these references, it is clearly demonstrated that the proposed simulation approach is suitable for the prediction of the precipitation kinetics of AlN in low alloy steel. The identical procedure is used for the present ultra low carbon steel. According to our expectation, AlN precipitation is predicted to occur only at austenite grain boundaries for temperatures higher than 900 °C.

In the present work, the experimental TEM analysis provides some information on the size and morphology of AlN precipitates (Figs. 2(b-f) and 3(b-f)) in ultra-low C steel along with the corresponding precipitation kinetics data. Unfortunately, no quantitative experimental data of precipitate sizes can be provided, since the precipitates show rather complex morphologies and they are not homogeneously distributed in the inspected volumes. However, the figures demonstrate qualitatively the evolution of the precipitate sizes with increasing annealing time. The order of magnitude of the mean radii of the experimentally observed precipitates coincides well with the corresponding calculations shown in Figs. 2(a) and 3(a). Moreover, Fig. 6 demonstrates that the calculation of the TTP diagram is in good agreement with the experimental measurement, since the $t_{0.05}$ curve corresponds very well with the detection limit of AlN precipitates found in TEM.

## Summary

AlN precipitation is investigated in the austenite region of ultra low carbon steel. Experimental investigations are carried out after isothermal annealing of the alloy at two different temperatures of 1050 °C and 950 °C and various annealing times. TEM thin foils analyses are performed for the characterization of the size and the morphology of the AlN particles. Various different structures are observed, covering cuboids, large plates as well as irregularly shaped particles. In addition to the experimental investigations, thermo-kinetic simulations are carried out using the software package MatCalc, providing kinetic information on the precipitation process. The simulations predict that, in the present alloy, AlN precipitation occurs predominantly at grain boundaries, whereas precipitation at dislocations is only predicted at temperatures below 900 °C. The nose temperature for AlN precipitation in the austenite region of the present alloy is observed at approximately 1050 °C and $t_{0.05}$ at this temperature is about 20 s. The prediction of the precipitation kinetics of AlN is in good agreement with the experimentally determined data.

## References

[1] T. Gladman: The Physical Metallurgy of Microalloyed Steels, The Institute of Materials, London, UK, 1997.
[2] M. P. Sidey: Iron and Steel, 40 (1967), 168.
[3] E. L. Brown, A. J. DeArdo: Aluminium Nitride Precipitation in C-Mn-Si and Microalloyed Steels, Proc. of the conference 'Thermo-mechanical Processing of microalloyed Austenite', eds. A. J. DeArdo, G. A. Ratz, and P. J. Wray, The Metallurical Society of AIME, Warrendale, PA, USA, 1982, 319.
[4] J. R. Wilcox, R. W. K. Honeycombe: Mater. Sci. Technol., 3 (1987), 849.
[5] L. M. Cheng, E. B. Hawbolt, T. R. Meadowcroft: Canadian Metallurgical Quaterly, (39) 2000, 73.
[6] J. F. Chávez-Alcalá, A. Rodríguez-Reyes, E. G. Navarrete-Ramos, H. J. Dorantes-Rosales, M. L. Saucedo-Munoz, V. M. López-Hirata: ISIJ International, (41) 2001, 1532.
[7] S. Hanai, N. Takemoto, Y. Mizuyama: Trans. ISIJ, 11 (1971), 24.
[8] G. R. Speich, J. Cuddy, C. R. Gordan, A. J. DeArdo: Formation of Ferrite From Control-Rolled Austenite, Proc. of the conference 'Phase Transformations in Ferrous Alloys', eds. A. R. Marderm, and J. I. Goldstein, The Metallurgical Society of AIME, Warrendale, PA, USA, 1984, 341.
[9] T. Gladman, F. B. Pickering: J. Iron Steel Inst., 205 (1967), 653.
[10] K. J. Irvine, F. B. Pickering, T. Gladman: J. Iron Steel Inst., 205 (1967), 161.
[11] T. Gladman: Heat Treatment of Metals, 21 (1994), 11.
[12] B. Mintz, J. R. Wilcox, D. N. Crowther: Mater. Sci. Technol., 2 (1986), 589.
[13] R. Abushosha, S. Ayyad, B. Mintz: Mater. Sci. Technol., 14 (1998), 346.
[14] L. A. Erasmus: J. Iron Steel Inst., 202 (1964), 32.
[15] V. Massardier, V. Guétaz, J. Merlin, M. Solar: Mater. Sci. Forum, 426–432. (2003), 1267.
[16] F. G. Wilson, T. Gladman: Int. Mater. Rev., 33 (1988), 221.
[17] E. T. Turkdogan: Iron and Steelmaker, 16 (1989), 61.
[18] B. Mintz, S. Yue, J. J. Jonas: Int. Mater. Rev., 36 (1991), 187.
[19] K. E. Höner, S. Baliktay: Gießerei-Forschung, 30 (1978), 53.
[20] F. K. Naumann, und H. Erich, Stahl und Eisen, 82 (1962), 612.
[21] K. Roesch, und K. Zimmermann, Stahlguss, BT Band 17 aus der Reihe Stahleisen-Bücher, Verlag Stahleisen GmbH, Düsseldorf, Germany, 1966.

  

[22] K. Schwerdtfeger: Rißanfälligkeit von Stählen beim Stranggießen und Warmumformen, Verlag Stahleisen GmbH, Düsseldorf, Germany, 1994.
[23] D. E. Dutcher: Modern Casting, 89 (1999), 46.
[24] P. Heritier, A. Fourdeux, A. Kobylanski: Scripta Metallurgica, 15 (1981), 753.
[25] V. Massardier, V. Guétaz, J. Merlin, M. Solar: Mater. Sci. Eng. A, 355 (2003), 299.
[26] R. Ogawa, T. Fukutsuka, Y. Yagi: Trans. ISIJ, 12 (1972), 291.
[27] M. H. Biglari, C. M. Brakman, E. J. Mittemeijer, S. Van Der Zwaag: Metall. Mater. Trans. A, 26 (1995), 765.
[28] M. Sennour, C. Esnouf: Acta Mater., 51 (2003), 943.
[29] R. Radis, E. Kozeschnik: Modelling Simul. Mater. Sci. Eng., 18 (2010), 055003.
[30] H. F. Beeghly: Analytical Chemistry, 21 (1949), 1513.
[31] E. Kozeschnik, J. Svoboda, R. Radis, F. D. Fischer: Modelling Simul. Mater. Sci. Eng., 18 (2010), 015011.
[32] J. Svoboda, F. D. Fischer, P. Fratzl, E. Kozeschnik: Mater. Sci. Eng., A385 (2004), 166.
[33] E. Kozeschnik, J. Svoboda, P. Fratzl, F. D. Fischer: Mater. Sci. Eng., A385 (2004), 157.
[34] E. Kozeschnik, J. Svoboda, F. D. Fischer: CALPHAD, 28 (2005), 379.
[35] Thermodynamic Database 'mc_steel', version 1.50, Institute of Materials Science and Technology, Vienna University of Technology.
[36] Diffusion Database 'mc_sample_fe', version 1.03, Institute of Materials Science and Technology, Vienna University of Technology.
[37] K. G. F. Janssens, D. Raabe, E. Kozeschnik, M. A. Miodownik, B. Nestler: Computational Materials Engineering – An Introduction to Microstructure Evolution, Elsevier Academic Press, Oxford, UK, 2007, 179–217.
[38] K. Russell: Adv. Colloid Sci., 13 (1980), 205.
[39] E. Kozeschnik, J. Svoboda, F. D. Fischer: On the Role of Chemical Composition in Multi-Component Nucleation, Proc Int. Con. on 'Solid-Solid Phase Transformations in Inorganic Materials (PTM 2005)', Pointe Hilton Squaw Peak Resort, Phoenix, AZ, USA, 2005, 301.
[40] B. Sonderegger, E. Kozeschnik: Metall. Mater. Trans., 40A (2009), 499.
[41] B. Sonderegger, E. Kozeschnik: Scripta Mater., 60 (2009), 635.
[42] R. Radis, M. Schaffer, M. Albu, G. Kothleitner, P. Pölt, E. Kozeschnik: Acta Mater., 57 (2009), 5739.
[43] R. Kampmann, R. Wagner: Kinetics of Precipitation in Metastable Binary Alloys - Theory and Applications to Cu-1.9 at% Ti and Ni-14 at% Al, Proc. of the '2nd Acta-Scripta Metallurgica Conference', Sonnenberg, Germany, 1983, 91.
[44] D. Hull, D. J. Bacon: Introduction to Dislocations, Pergamon Press Ltd., Oxford, UK, 1984.
[45] P. Villars, L. D. Calvert: Pearson's Handbook of Crystallographic Data for Intermetallic Phases, ASM International, Vol. 1, Second Edition, Materials Park, Ohio, USA, 1996.

  